Prompt hadroproduction of $\eta_c(1S, 2S)$ in the k_T-factorization approach

Izabela Babiarz,[a] **Roman Pasechnik,**[b,c] **Wolfgang Schäfer**[a] **and Antoni Szczurek**[a,d]

[a] *Institute of Nuclear Physics, Polish Academy of Sciences,*
ul. Radzikowskiego 152, PL-31-342 Kraków, Poland

[b] *Department of Astronomy and Theoretical Physics,*
Lund University, SE-223 62 Lund, Sweden

[c] *Nuclear Physics Institute ASCR,*
25068 Rež, Czech Republic

[d] *College of Natural Sciences, Institute of Physics,*
University of Rzeszów, ul. Pigonia 1, PL-35-310 Rzeszów, Poland

E-mail: izabela.babiarz@ifj.edu.pl, roman.pasechnik@thep.lu.se,
wolfgang.schafer@ifj.edu.pl, antoni.szczurek@ifj.edu.pl

ABSTRACT: In this work, we present a thorough analysis of $\eta_c(1S, 2S)$ quarkonia hadroproduction in $k_\perp$-factorisation in the framework of the light-front potential approach for the quarkonium wave function. The off-shell matrix elements for the $g^*g^*\eta_c(1S, 2S)$ vertices are derived. We discuss the importance of taking into account the gluon virtualities. We present the transverse momentum distributions of η_c for several models of the unintegrated gluon distributions. Our calculations are performed for four distinct parameterisations for the $c\bar{c}$ interaction potential consistent with the meson spectra. We compare our results for $\eta_c(1S)$ to measurements by the LHCb collaboration and present predictions for $\eta_c(2S)$ production.

Contents

1 Introduction

The quarkonia production reactions in hadronic collisions at the Large Hadron Collider (LHC) continue to attract a lot of interest [1]. In this paper, we concentrate on the direct hadroproduction of the ground state of the charmonium family, $\eta_c(1S)$, and its first excited state $\eta_c(2S)$. Both are pseudoscalar particles of even charge parity $J^{PC} = 0^{-+}$. Like other C-even quarkonia, the dominant production mechanism is through the $gg \to \mathcal{Q}$ gluon fusion $2 \to 1$ process. In the standard collinear-factorization approach one must go to next-to-leading order (NLO) approximation to calculate the transverse momentum distribution of a given quarkonium state and include $2 \to 2$ processes like $gg \to \mathcal{Q}g$. In the k_T-factorization approach [2–7], the transverse momentum of the quarkonium originates from the transverse momenta of incident virtual gluons entering the hard $g^*g^* \to \mathcal{Q}$ process. The k_T-factorization approach is especially appropriate in the high-energy kinematics, where partons carry small momentum fractions x of the incoming protons, often discussed in the framework of the BFKL formalism [8–11]. In our calculations we will adopt the color-singlet model, which treats the quarkonium as a two-body bound state of a heavy quark and antiquark. Such a formalism was used previously for the production of χ_{cJ} $(J = 0, 1, 2)$ quarkonia (see e.g. ref. [12]), and a relatively good agreement with data was obtained from an unintegrated gluon distribution (UGD), which effectively includes the higher-order contributions.

Recently, the LHCb collaboration has measured the transverse momentum distributions of η_c in the $p\bar{p}$ decay channel [13] (see also the recent PhD thesis [14]). The experimental method allows to measure η_c charmonia only for $p_T > 6.5\,\mathrm{GeV}$. In the present study, we will discuss production of $\eta_c(1S)$ and $\eta_c(2S)$ also at lower transverse momenta. This is a region where the effects of nonlinear evolution for the UGDs may potentially show up. This was discussed briefly in ref. [12] in the context of low transverse momentum χ_c production.

A crucial ingredient of our k_T-factorization approach is the off-shell matrix element for the $g^*g^* \to \eta_c$ transition. Recently in ref. [15] we discussed in detail the $\gamma^*\gamma^* \to \eta_c(1S, 2S)$ form factors. These form factors were calculated there from the $c\bar{c}$ light-front (LF) wave functions obtained from different $c\bar{c}$ interaction potentials obtained in ref. [16]. In the present paper, we will apply the formalism developed in ref. [15] using the potential approach and the Melosh spin transform to derive the proper LF wave functions of the $\eta_c(1S, 2S)$ states.[1] Here, we employ the same LF formalism for computation of the $g^*g^* \to \eta_c$ vertex, for both gluons being off-shell. We wish to demonstrate the role of the form factor and to estimate the uncertainties for the η_c production yields related to it. This was not discussed so far in the context of quarkonia production in proton-proton collisions. We wish to focus also on a possibility of testing the unintegrated gluon distributions by comparing our predictions to the experimental data.

Previously, the prompt $\eta_c(1S)$ production was discussed in various factorization approaches: collinear factorization [18–22], the TMD-factorization with transverse momentum dependent distributions of on-shell gluons, and on-shell matrix elements [23, 24], and the k_T-factorization in ref. [25]. So far, the $\eta_c(2S)$ production process was discussed only in the collinear factorization approach in ref. [26].

The paper is organised as follows. In section 2, we discuss the formalism behind the quarkonia hadroproduction processes in the k_T-factorization approach. In section 3 we present the most relevant numerical results for the differential $\eta_c(1S, 2S)$ production cross sections versus the available experimental data and discuss the related theoretical uncertainties. The basic concluding remarks and the main results are summarised in section 4.

2 Formalism

2.1 Off-shell matrix element and cross section

In figure 1 we show a generic Feynman diagram for $\eta_c(1S)$ quarkonium production in proton-proton collision via gluon-gluon fusion. This diagram illustrates the situation adequate for the k_T-factorization calculations used in the present paper. The inclusive cross section for η_c-production via the $2 \to 1$ gluon-gluon fusion mode is obtained from

$$d\sigma = \int \frac{dx_1}{x_1} \int \frac{d^2\boldsymbol{q}_1}{\pi \boldsymbol{q}_1^2} \mathcal{F}(x_1, \boldsymbol{q}_1^2, \mu_F^2) \int \frac{dx_2}{x_2} \int \frac{d^2\boldsymbol{q}_2}{\pi \boldsymbol{q}_2^2} \mathcal{F}(x_2, \boldsymbol{q}_2^2, \mu_F^2) \frac{1}{2x_1 x_2 s} \overline{|\mathcal{M}|^2} \, d\Phi(2 \to 1). \tag{2.1}$$

The unintegrated gluon distributions are normalized such, that the collinear glue is obtained from

$$xg(x, \mu_F^2) = \int^{\mu_F^2} \frac{d\boldsymbol{k}^2}{\boldsymbol{k}^2} \mathcal{F}(x, \boldsymbol{k}^2, \mu_F^2), \tag{2.2}$$

where from now on we will no longer show the dependence on the factorization scale μ_F^2 explicitly.

---

[1]For a recent analysis of the role of the Melosh spin transform in vector S-wave meson photoproduction with and without D-wave admixture, see ref. [17].
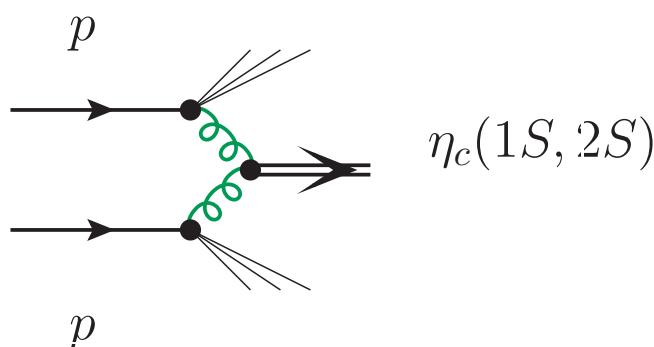
Figure 1. Generic diagram for the inclusive process of $\eta_c(1S)$ or $\eta_c(2S)$ production in proton-proton scattering via two gluons fusion.

Let us denote the four-momentum of the η_c by p and parametrize it in light-cone coordinated as

$$p = (p_+, p_-, \boldsymbol{p}) = \left(\frac{m_T}{\sqrt{2}} e^y, \frac{m_T}{\sqrt{2}} e^{-y}, \boldsymbol{p} \right), \qquad (2.3)$$

where we introduced the transverse mass

$$m_T = \sqrt{\boldsymbol{p}^2 + M_{\eta_c}^2}, \qquad (2.4)$$

where M_{η_c} is the mass of the η_c-meson, and y is its rapidity in the pp cms-frame. The phase-space element is

$$d\Phi(2 \to 1) = (2\pi)^4 \delta^{(4)}(q_1 + q_2 - p) \frac{d^4 p}{(2\pi)^3} \delta(p^2 - M_{\eta_c}^2). \qquad (2.5)$$

In the k_T-factorization approach, gluons are off-shell, $q_i^2 = -\boldsymbol{q}_i^2$, and their four momenta are written as ($\sqrt{s}$ is the pp center-of-mass energy):

$$q_1 = (q_{1+}, 0, \boldsymbol{q}_1), \qquad q_2 = (0, q_{2-}, \boldsymbol{q}_2), \qquad (2.6)$$

with

$$q_{1+} = x_1 \sqrt{\frac{s}{2}}, \qquad q_{2-} = x_2 \sqrt{\frac{s}{2}}. \qquad (2.7)$$

We can then calculate the phase-space element as

$$d\Phi(2 \to 1) = \frac{2\pi}{s} \delta\left(x_1 - \frac{m_T}{\sqrt{s}} e^y \right) \delta\left(x_2 - \frac{m_T}{\sqrt{s}} e^{-y} \right) \delta^{(2)}(\boldsymbol{q}_1 + \boldsymbol{q}_2 - \boldsymbol{p}) \, dy \, d^2\boldsymbol{p}. \qquad (2.8)$$

We therefore obtain for the inclusive cross section

$$\frac{d\sigma}{dy d^2 \boldsymbol{p}} = \int \frac{d^2 \boldsymbol{q}_1}{\pi \boldsymbol{q}_1^2} \mathcal{F}(x_1, \boldsymbol{q}_1^2) \int \frac{d^2 \boldsymbol{q}_2}{\pi \boldsymbol{q}_2^2} \mathcal{F}(x_2, \boldsymbol{q}_2^2) \, \delta^{(2)}(\boldsymbol{q}_1 + \boldsymbol{q}_2 - \boldsymbol{p}) \frac{\pi}{(x_1 x_2 s)^2} \overline{|\mathcal{M}|^2}, \qquad (2.9)$$

where the momentum fractions of gluons are fixed as $x_{1,2} = m_T \exp(\pm y)/\sqrt{s}$. The off-shell matrix element is written in terms of the Feynman amplitude as (we restore the color-indices):

$$\mathcal{M}^{ab} = \frac{q_{1\perp}^{\mu} q_{2\perp}^{\nu}}{|\boldsymbol{q}_1||\boldsymbol{q}_2|} \mathcal{M}_{\mu\nu}^{ab} = \frac{q_{1+}q_{2-}}{|\boldsymbol{q}_1||\boldsymbol{q}_2|} n^{+\mu} n^{-\nu} \mathcal{M}_{\mu\nu}^{ab} = \frac{x_1 x_2 s}{2|\boldsymbol{q}_1||\boldsymbol{q}_2|} n^{+\mu} n^{-\nu} \mathcal{M}_{\mu\nu}^{ab}. \qquad (2.10)$$

In covariant form, the matrix element reads:

$$\mathcal{M}_{\mu\nu}^{ab} = (-i)4\pi\alpha_s\, \varepsilon_{\mu\nu\alpha\beta} q_1^{\alpha} q_2^{\beta} \frac{\mathrm{Tr}[t^a t^b]}{\sqrt{N_c}}\, I(\boldsymbol{q}_1^2, \boldsymbol{q}_2^2). \qquad (2.11)$$

Notice that it fulfills the gauge-invariance constraints

$$q_1^{\mu}\mathcal{M}_{\mu\nu}^{ab} = q_2^{\nu}\mathcal{M}_{\mu\nu}^{ab} = 0, \qquad (2.12)$$

which we used in trading the effective polarizations proportional to $q_{i\perp}^{\mu}$ to $n_{\mu}^{\pm}$.[2]

To the lowest order, it is proportional to the matrix element for the $\gamma^*\gamma^*\eta_c$ vertex. In particular, the form factor $I(\boldsymbol{q}_1^2, \boldsymbol{q}_2^2)$ is related to the $\gamma^*\gamma^*\eta_c$ transition form factor $F(Q_1^2, Q_2^2)$, $Q_i^2 = \boldsymbol{q}_i^2$ as

$$F(Q_1^2, Q_2^2) = e_c^2 \sqrt{N_c}\, I(\boldsymbol{q}_1^2, \boldsymbol{q}_2^2), \qquad (2.13)$$

and it can be represented in terms of the LF wave function as

$$I(\boldsymbol{q}_1^2, \boldsymbol{q}_2^2) = 4m_c \int \frac{dz d^2\boldsymbol{k}}{z(1-z)16\pi^3} \psi(z, \boldsymbol{k}) \left\{ \frac{1-z}{(\boldsymbol{k} - (1-z)\boldsymbol{q}_2)^2 + z(1-z)\boldsymbol{q}_1^2 + m_c^2} \right. \qquad (2.14)$$
$$\left. + \frac{z}{(\boldsymbol{k} + z\boldsymbol{q}_2)^2 + z(1-z)\boldsymbol{q}_1^2 + m_c^2} \right\}.$$

For details of the derivation and the normalization conventions and relation to the potential model wave function of the LF radial wave function $\psi(z, \boldsymbol{k})$, see ref. [15]. In this work, we will use the calculations of the form factor which were obtained in [15]. There, the representation of the $\gamma^*\gamma^*\eta_c$ transition form factor in terms of the LF wave function of the η_c was derived. Several wave-functions obtained from potential models for the $c\bar{c}$ system which were previously obtained in ref. [16] were used.

In ref. [15] we also studied the NRQCD limit, where relative motion of quark and antiquark are neglected. This amounts to $\psi(z, \boldsymbol{k}) \propto \delta(z - \frac{1}{2})\delta^{(2)}(\boldsymbol{k})$ and leads to the transition form factor

$$F_{\mathrm{NRQCD}}(Q_1^2, Q_2^2) = \frac{4e_c^2\sqrt{N_c}}{\sqrt{\pi M_{\eta_c}}} \frac{1}{M_{\eta_c}^2 + Q_1^2 + Q_2^2}\, R(0), \qquad (2.15)$$

where $R(0)$ is the value of the potential-model radial wave function at the spatial origin.

---

[2]In the BFKL formalism involving the reggeized gluons [10, 11] one would indeed derive the Feynman-rules for off-shell gluons with polarizations $n_{\mu}^{\pm}$. The translation to $q_{i\perp}^{\mu}$ is more convenient in comparing to on-shell or collinear approaches.

Inserting the explicit form of the matrix element

$$
\begin{aligned}
n^{+\mu}n^{-\mu}\mathcal{M}^{ab}_{\mu\nu} &= 4\pi\alpha_s(-i)[\boldsymbol{q}_1,\boldsymbol{q}_2]\frac{\mathrm{Tr}[t^a t^b]}{\sqrt{N_c}}I(\boldsymbol{q}_1^2,\boldsymbol{q}_2^2) \\
&= 4\pi\alpha_s(-i)\frac{1}{2}\delta^{ab}\frac{1}{\sqrt{N_c}}[\boldsymbol{q}_1,\boldsymbol{q}_2]\,I(\boldsymbol{q}_1^2,\boldsymbol{q}_2^2)\,,
\end{aligned}
\tag{2.16}
$$

and averaging over colors, we obtain our final result:

$$
\begin{aligned}
\frac{d\sigma}{dyd^2\boldsymbol{p}} = \int\frac{d^2\boldsymbol{q}_1}{\pi\boldsymbol{q}_1^4}\mathcal{F}(x_1,\boldsymbol{q}_1^2)\int\frac{d^2\boldsymbol{q}_2}{\pi\boldsymbol{q}_2^4}\mathcal{F}(x_2,\boldsymbol{q}_2^2)\,\delta^{(2)}(\boldsymbol{q}_1+\boldsymbol{q}_2-\boldsymbol{p}) \\
\times\frac{\pi^3\alpha_s^2}{N_c(N_c^2-1)}|[\boldsymbol{q}_1,\boldsymbol{q}_2]\,I(\boldsymbol{q}_1^2,\boldsymbol{q}_2^2)|^2\,.
\end{aligned}
\tag{2.17}
$$

Parametrizing the transverse momenta as $\boldsymbol{q}_i = (q_i^x, q_i^y) = |\boldsymbol{q}_i|(\cos\phi_i, \sin\phi_i)$, we can write the vector product $[\boldsymbol{q}_1, \boldsymbol{q}_2]$ as

$$
[\boldsymbol{q}_1, \boldsymbol{q}_2] = q_1^x q_2^y - q_1^y q_2^x = |\boldsymbol{q}_1||\boldsymbol{q}_2|\sin(\phi_1 - \phi_2)\,.
\tag{2.18}
$$

In our numerical calculations presented below, we set the factorization scale to $\mu_F^2 = m_T^2$, and the renormalization scale is taken in the form:

$$
\alpha_s^2 \to \alpha_s(\max\{m_T^2, \boldsymbol{q}_1^2\})\alpha_s(\max\{m_T^2, \boldsymbol{q}_2^2\})\,.
\tag{2.19}
$$

2.2 Normalization of the $g^* g^* \eta_c(1S, 2S)$ form factors

The normalization of the inclusive cross section depends crucially on the value of the $g^* g^* \eta_c$ form factor for vanishing gluon virtualities $\boldsymbol{q}_1^2 = \boldsymbol{q}_2^2 = 0$. The latter in turn is directly related to the $\eta_c \to gg$ decay width. From the proportionality of the $g^* g^* \eta_c$ and $\gamma^* \gamma^* \eta_c$ vertices to the leading order (LO), we obtain, that at LO, the $\gamma\gamma$ and gg widths are related by

$$
\Gamma_{\mathrm{LO}}(\eta_c \to gg) = \frac{N_c^2-1}{4N_c^2}\frac{1}{e_c^4}\left(\frac{\alpha_s}{\alpha_{\mathrm{em}}}\right)^2\Gamma_{\mathrm{LO}}(\eta_c \to \gamma\gamma)\,,
\tag{2.20}
$$

where the LO $\gamma\gamma$ width in turn is related to the transition form factor for vanishing virtualities through

$$
\Gamma_{\mathrm{LO}}(\eta_c \to \gamma\gamma) = \frac{\pi}{4}\alpha_{\mathrm{em}}^2 M_{\eta_c}^3|F(0,0)|^2\,.
\tag{2.21}
$$

At NLO, the expressions for the widths read (see e.g. [27, 28])

$$
\begin{aligned}
\Gamma(\eta_c \to \gamma\gamma) &= \Gamma_{\mathrm{LO}}(\eta_c \to \gamma\gamma)\left(1 - \frac{20-\pi^2}{3}\frac{\alpha_s}{\pi}\right)\,, \\
\Gamma(\eta_c \to gg) &= \Gamma_{\mathrm{LO}}(\eta_c \to gg)\left(1 + 4.8\frac{\alpha_s}{\pi}\right)\,.
\end{aligned}
\tag{2.22}
$$

In order to control the model uncertainty on the normalization, one may want to adjust its value $F(0,0)$ to the measured decay width. Here we face the ambiguity of fitting either

	Experimental values	Derived from eq. (2.22)
	Γ_{tot} (MeV) [32]	$|F(0,0)|_{gg}[GeV^{-1}]$
$\eta_c(1S)$	31.9±0.7	0.119±0.001
$\eta_c(2S)$	11.3±3.2±2.9	0.053±0.010

Table 1. Total decay widths as well as $|F(0,0)|$ obtained from Γ_{tot} using the next-to-leading order approximation (see eq. (2.22)).

	Experimental values	Derived from eq. (2.21)	Derived from eq. (2.22)
	$\Gamma_{\gamma\gamma}$(keV) [32]	$|F(0,0)|[GeV^{-1}]$	$|F(0,0)|_{\gamma\gamma}[GeV^{-1}]$
$\eta_c(1S)$	5.0 ±0.4	0.067±0.003	0.079±0.003
$\eta_c(2S)$	1.9 ±1.3 ·10^{-4} · $\Gamma_{\eta_c(2S)}$	0.033±0.012	0.038±0.014

Table 2. Radiative decay widths as well as $|F(0,0)|$ obtained from $\Gamma_{\gamma\gamma}$ using leading order and next-to-leading order approximation (see formulas eq. (2.21), (2.22)).

to the hadronic or to the $\gamma\gamma$ width. As there are no other known radiative decays besides $\gamma\gamma$, one may try to identify the gg-width with the total (hadronic) width.

In tables 1, 2, we show the values of $|F(0,0)|$ obtained in three different ways. In table 1 we show the result extracted from the total decay width. Here we use the strong coupling $\alpha_s = 0.26$, which is appropriate to our choice of the renormalization scale in the production amplitudes. In table 2 we extract the value of $|F(0,0)|$ from the radiative decay width in two different ways. The first result is obtained based on eq. (2.21) using the experimental value for $\Gamma(\eta_c \to \gamma\gamma)$ on the left hand side, while the second one uses the NLO relation 2.22.

We observe a substantial difference between the two different extractions of $|F(0,0)|$. While in the $\eta_c(2S)$ case, the error bars are too large to claim an inconsistency, the situation for the $\eta_c(1S)$ is not satisfactory. This is in fact an old problem and may hint at an insufficiency of the potential model treatment of the η_c. Various possible solutions have been proposed, such as an admixture of light hadron states [29], a mixing with a pseudoscalar glueball [30], or nonperturbative instanton effects in the hadronic decay [31].

2.3   Unintegrated gluon distributions

We use a few different UGDs which are available from the literature, e.g. from the TMDLib package [33] or the CASCADE Monte Carlo code [34].

1. Firstly we use a glue constructed according to the prescription initiated in [35] and later updated in [36, 37], which we label below as "KMR". It uses as an input the collinear gluon distribution from [38].

2. Secondly, we employ two UGDs obtained by Kutak in [39]. There are two versions of this UGD. Both introduce a hard scale dependence via a Sudakov form factor into solutions of a small-x evolution equation. The first version uses the solution of a
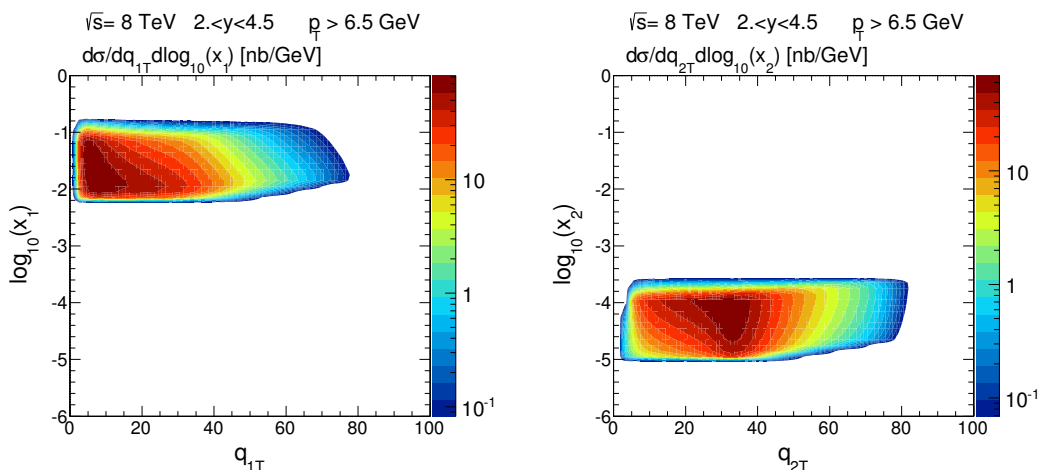
Figure 2. Two-dimensional distributions in (x_1, q_{1T}) (left panel) and in (x_2, q_{2T}) (right panel) for $\eta_c(1S)$ production for $\sqrt{s} = 8\,\text{TeV}$. In this calculation the KMR UGD was used for illustration.

linear, BFKL [8, 9] evolution with a resummation of subleading terms and is denoted by "Kutak (linear)". The second UGD, denoted as "Kutak (nonlinear)" uses instead a nonlinear evolution equation of Balitsky-Kovchegov [40–42] type. Both of the Kutak's UGDs can be applied only in the small-x regime, $x < 0.01$.

3. The third type of UGD which we use has been obtained by Hautmann and Jung [43] from a description of precise HERA data on deep inelastic structure function by a solution of the CCFM evolution equations [44–46]. We use "Set 2" of ref. [43].

For the case of the KMR UGD, it has recently been shown in [47], that it includes effectively also higher order corrections of the collinear factorization approach. In this sense should give within our approach a result similar to that found recently in the NLO approach [22] at not too small transverse momenta. In contrast to the collinear NLO approach in our approach we can go to very small transverse momenta close to $p_T = 0$.

3 Numerical results

Before presenting results for the cross sections let us understand first the kinematical situation relevant for the LHCb experiment. The gluons entering the $g^*g^* \to \chi_c$ vertex (see figure 1) are characterized by their longitudinal fractions (x_1 or x_2) or gluon virtualities at high-energies directly related to the their transverse momenta $\boldsymbol{q}_{1,2}$. In figure 2 we show two dimensional distributions for the first gluon ($x_1, q_{1T} = |\boldsymbol{q}_1|$) (left panel) and for the second gluon ($x_2, q_{2T} = |\boldsymbol{q}_2|$) (right panel). We observe a large asymmetry of the two distributions related to asymmetric LHCb configuration: $y \in (2, 4.5)$. The relatively large lower cut on η_c transverse momentum $p_T > 6.5\,\text{GeV}$ causes that q_{1T} and q_{2T} are themselves not small and are essentially in the perturbative regime where UGDs should be rather reliable. Moreover, large p_T of the η_c also entails the large factorization scale. In this calculation we used the KMR UGD described above.
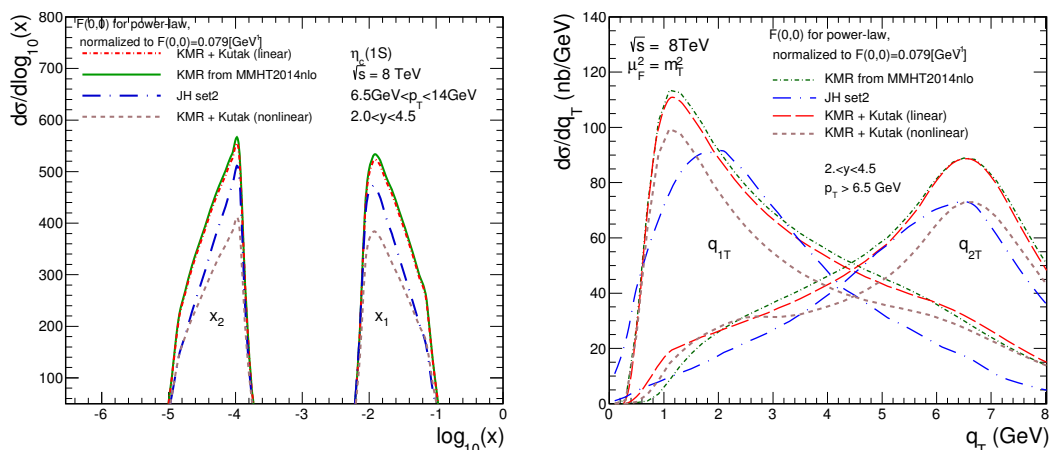
Figure 3. Distributions in $\log_{10}(x_1)$ or $\log_{10}(x_2)$ (left panel) and distributions in q_{1T} or q_{2T} (right panel) for the LHCb kinematics. Here the different UGDs were used in our calculations. Here we show an example, where $\sqrt{s} = 8\,\text{TeV}$.

The projections on the x_i and q_{iT} axes are shown in figure 3. The asymmetric LHCb kinematics causes that x_1 is rather large and x_2 is very small — even smaller than 10^{-5}, much smaller than for other perturbative partonic processes. We observe also a clear asymmetry in q_{1T} and q_{2T}. The q_{2T} transverse momenta corresponding to small x_2 are substantially larger than q_{1T} of the large-x_1 gluon. The low-x gluon therefore transfers the bulk of the transverse momentum of the η_c at large p_T.

We can exploit the good separation in $x_{1,2}$ to investigate the small-x behaviour of the unintegrated glue. From our choice of UGDs, the parametrizations of Kutak are available only for $x < 0.01$, so we will use these UGDs only for the small-x gluon. To avoid a proliferation of plots, we will use the Kutak UGDs always together with the KMR UGD for the large-x gluon. A similar strategy was taken previously in ref. [12].

The distributions for different UGDs in figure 3 are rather similar which makes our conclusions more universal.

Now we wish to show the behaviour of the different unintegrated gluon distribution on gluon transverse momentum k_T^2 for small $x_2 = 10^{-5}$ and typical scale parameter $\mu^2 = 100\,\text{GeV}^2$ relevant for the LHCb experiment. In the left panel of figure 4 we plot $\mathcal{F}(x, \boldsymbol{k}^2, \mu_F^2)/\boldsymbol{k}^2$, which corresponds to the distribution of the gluon transverse momentum squared $\boldsymbol{k}^2$. In the right panel the dimensionless UGD $\mathcal{F}(x, \boldsymbol{k}^2, \mu_F^2)$ is plotted. We show all the UGDs used in the present work. The left panel of figure 4 better shows the behaviour at smaller $\boldsymbol{k}^2 = k_T^2$, while the right panel emphasizes the large-k_T tails. We first observe, that the "linear" Kutak UGD looks quite similar to the KMR UGD, although both are constructed by different procedures. They have in common, that by their construction, both procedures lead to integrated gluon distributions which well describe jet cross sections at the LHC. The nonlinear Kutak UGD is considerably smaller than the linear one, especially at low transverse momenta. At very large transverse momenta the difference between linear and nonlinear UGDs becomes much smaller. The Jung-Hautmann distribution does not have an extended tail in k_T^2 as the other distributions, it is however much larger at low gluon transverse momenta. Can these different UGDs be tested in η_c production?
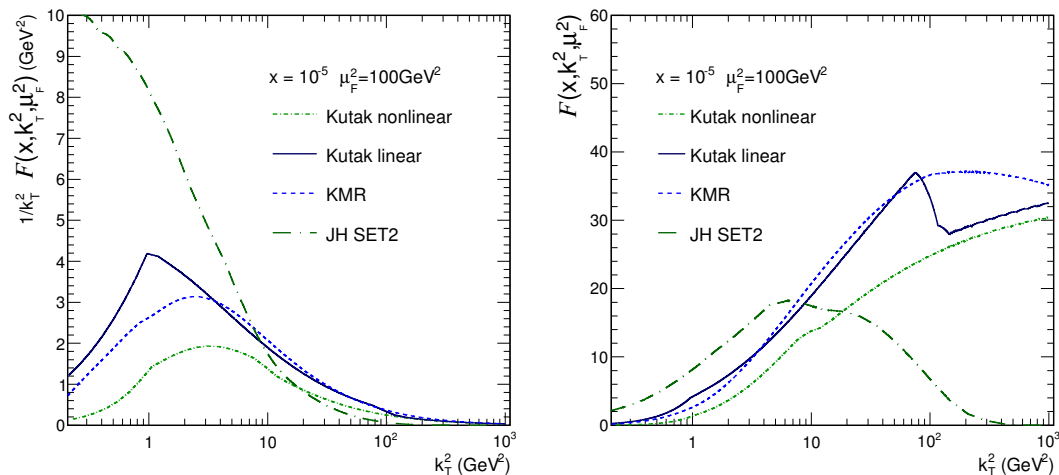
Figure 4. Unintegrated gluon densities for typical scale $\mu^2 = 100$ GeV^2 for $\eta_c(1S)$ production in proton-proton scattering at LHCb kinematics.

In figure 5 we compare the results of the k_T-factorization approach with the LHCb experimental data for $\sqrt{s} = 7$ and 8 TeV from ref. [13] and with the data for $\sqrt{s} = 13$ TeV from the recent PhD thesis [14].

The theoretical calculations use an off-shell form factor normalized to the $\gamma\gamma$-decay width at NLO. The off-shell $g^* g^* \eta_c$ form factor was calculated using the LF wave function obtained for one of the potentials (the so-called power-law potential) in [16]. It is up to the color factor proportional to the $\gamma^* \gamma^* \eta_c$ form factor obtained in [15]. The dependence on the choice of the potential will be discussed below.

The description of data for $\sqrt{s} = 7, 8$ TeV is reasonable for all UGDs. The theoretical results tend to be somewhat lower than the experimental data, especially at large p_T. The best description is obtained for the KMR UGD and the linear UGD by Kutak.

Our calculations fare a bit worse in the comparison to the data at $\sqrt{s} = 13$ TeV. Here all the UGDs give results substantially below the data.

As the data have fairly broad bins in p_T, in figure 6 we show the results for the KMR and Jung-Hautmann distributions also in a histogram represention which the reader may consider better suited for comparison with the LHCb experimental data.

Please note, that we include only the direct production mechanism in the color-singlet channel. A possible feed down from higher resonances, e.g. from the $h_c \to \eta_c \gamma$ radiative decay, is not included. See the recent ref. [25] for an estimate which finds a few percent contribution from the feed down. We also do not include a possible color-octet contribution. Finally, let us comment that some versions of k_T-factorization, e.g. [25], use a different formula for calculation of the inclusive cross section from UGD and off-shell matrix element, replacing the "flux-factor" $F = 2x_1 x_2 s$ in eq. (2.1) by a different expression with the same on-shell limit. We insist that our choice is consistent with the Feynman rules derived for reggeized off-shell gluons [10, 11]. We have checked, that with the expression used in [25], our results in the LHCb kinematics would decrease by $\approx 20 - 30\%$.

In general the difference between different UGDs is the largest at low p_T. Here one may e.g. expect effects related to nonlinear evolution and gluon saturation. While it is true
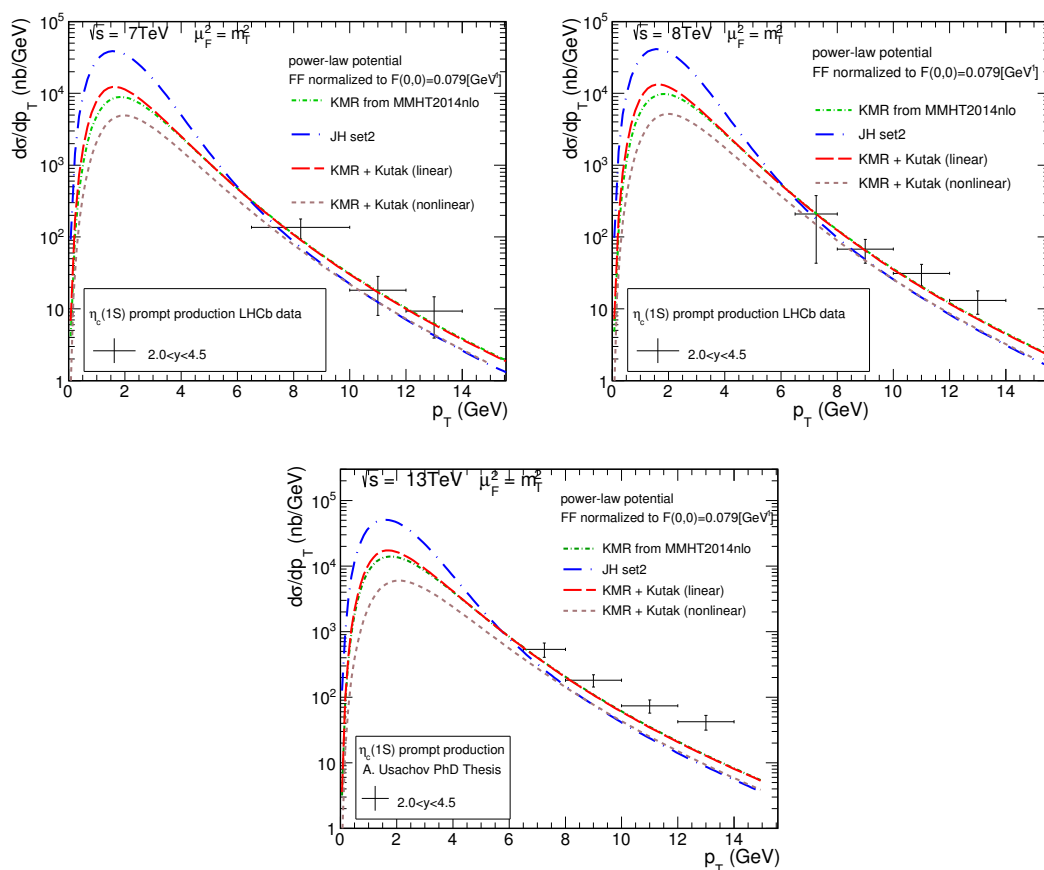
Figure 5. Differential cross section as a function of transverse momentum for prompt $\eta_c(1S)$ production compared with the LHCb data [13] for $\sqrt{s} = 7, 8\,\text{TeV}$ and preliminary experimental data [14] for $\sqrt{s} = 13\,\text{TeV}$. Different UGDs were used. Here we used the $g^*g^* \to \eta_c(1S)$ form factor calculated from the power-law potential.

that the cross section peaks precisely in this most interesting region around $p_T \sim 2\,\text{GeV}$ it seems to be exceedingly difficult to measure at $p_T < 6\,\text{GeV}$. At least this is true in the $p\bar{p}$ decay channel used by the LHCb collaboration. Perhaps other decay channels would be better in this respect. The $\gamma\gamma$ channel seems interesting as another option. A simulation of the signal and background would be valuable in this context.

When looking at the different UGDs in figure 4 one observes, that the Jung-Hautmann distribution stands out in that it does not have an extended tail at $\boldsymbol{k}^2 \gg \mu^2$. Does that have an effect on the large-p_T tail of the η_c cross section? In figure 7 we show the transverse momentum distribution in a somewhat broader range of η_c transverse momentum. We show our results for both LHCb and ATLAS/CMS kinematics. The cross section for ATLAS/CMS kinematics is somewhat larger than that for the LHCb kinematics, independently from the UGD used. Although the Jung-Hautmann UGD leads to a different shape of the p_T-distribution, there is no dramatic effect, such as a cutoff or break at very large p_T. This is due to the fact, that p_T enters the hard scale μ, and gluon transverse momenta much above the hard scale are not dominant.
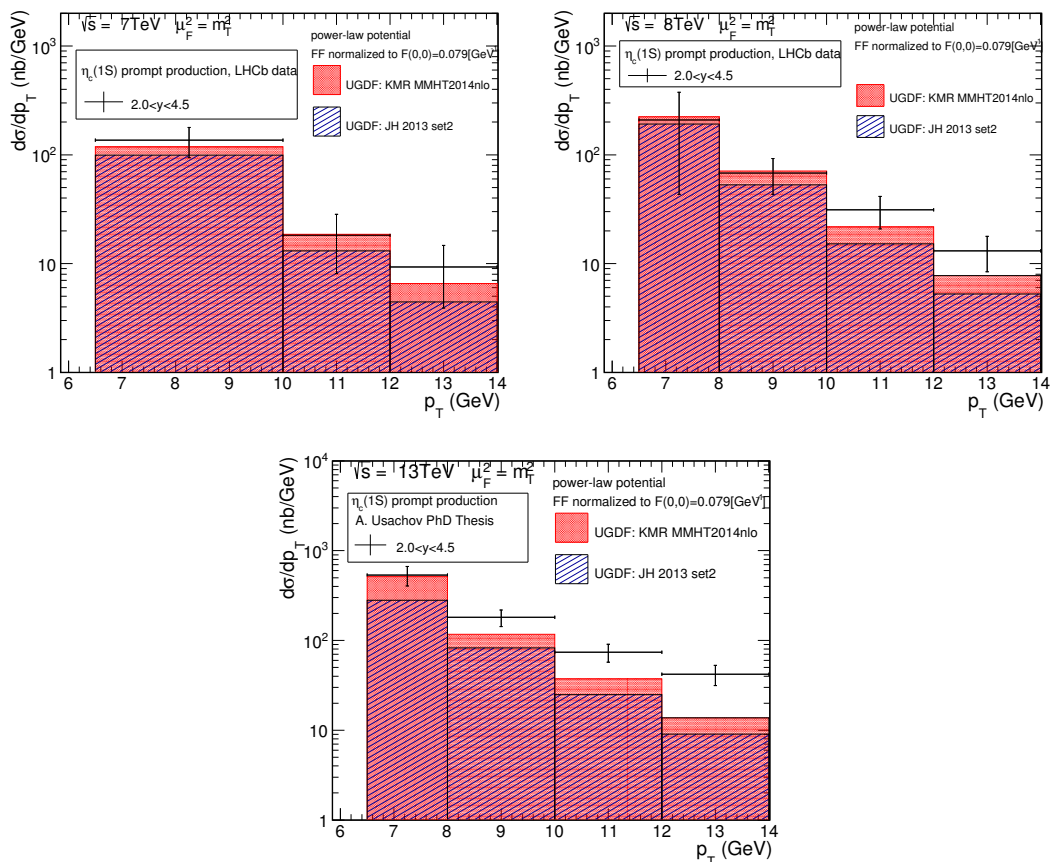
Figure 6. Prompt production differential cross section for $\eta_c(1S)$ compared with the LHCb data [13] for $\sqrt{s} = 7, 8\,\text{TeV}$ and preliminary experimental data [14] for $\sqrt{s} = 13\,\text{TeV}$.
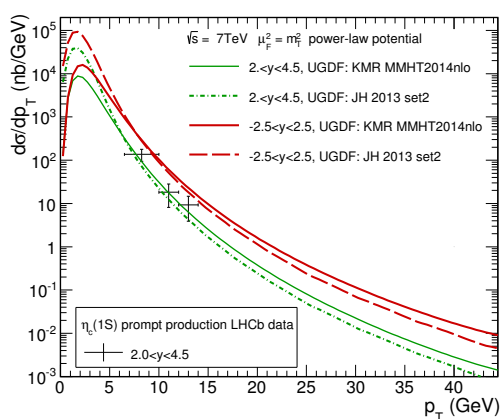

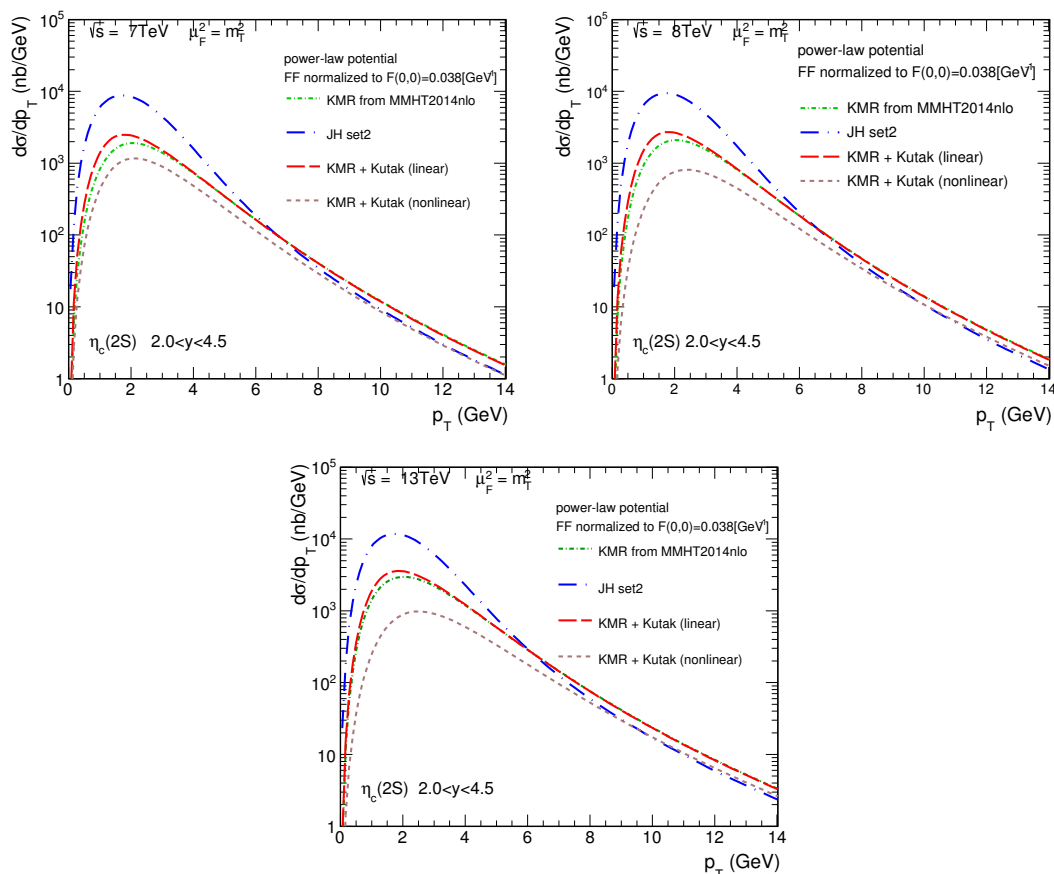**Figure 7**. Differential cross section for prompt $\eta_c(1S)$ production in a broad range of transverse momentum.

Figure 8. Differential cross section as a function of transverse momentum for prompt $\eta_c(2S)$ production for $\sqrt{s} = 7, 8, 13 \, \text{TeV}$.

In figure 8 we show our predictions for the so far unmeasured (at the LHC) $\eta_c(2S)$. In this calculation we also adjusted the value of $|F(0,0)|$ to the $\gamma\gamma$ width at NLO. The cross section is in a similar ballpark as for $\eta_c(1S)$ and the results for different UGDs show a similar variation as for the $\eta_c(1S)$ production.

We now wish to turn to the dependence of our results on the $c\bar{c}$ potential used for the calculation of the LF wave function. In ref. [15] the $\gamma^*\gamma^* \rightarrow \eta_c(1S, 2S)$ transition form factors, which is closely related to the $g^*g^*\eta_c(1S, 2S)$ form factors were obtained for different $c\bar{c}$ potentials. In figure 9 we show our results for different wave functions ($c\bar{c}$ potentials). To compare the influence the different wave functions have on the shape of the cross section, the respective form factors at the on-shell point, $|F(0,0)|$ were all adjusted to the same value dictated by the NLO expression for the experimental $\eta_c(1S, 2S) \rightarrow \gamma\gamma$ decay width.

In figure 10 we relax the normalization to the values predicted by the different potentials. Here the spread of results is bigger than in the previous case. We need to caution the reader, that generally the results from the phenomenological potentials undershoot the experimental widths. However, we wish to notice that experimental decay widths are known only with some precision [32]. In [48] a different values was measured. It appears,
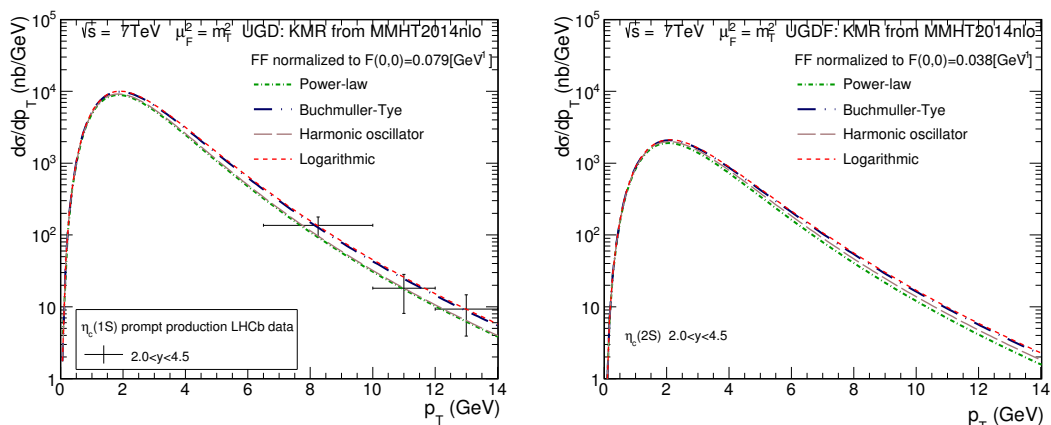
Figure 9. Transverse momentum distributions calculated with several different form factors obtained from different potential models of quarkonium wave function and one common normalization of $|F(0,0)|$ as explained in the text.
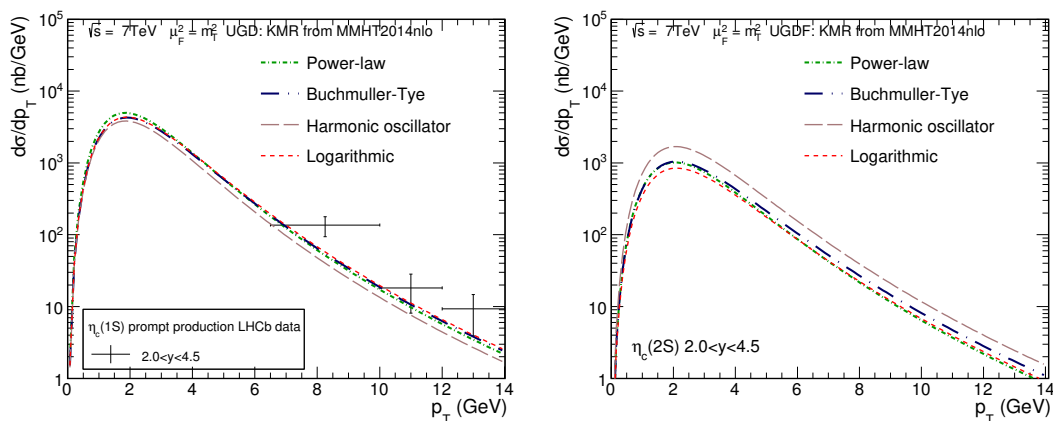

Figure 10. Distributions calculated with several different form factors obtained from different potential models of quarkonium.

that the behaviour of the off-shell form factors at large $\boldsymbol{q}_i^2$ is a more reliable result than their value at the on-shell point, though.

Finally it is interesting to discuss the NRQCD result, using the $g^* g^* \to \eta_c$ form factor from eq. (2.15). In figure 11 we show our results for $\eta_c(1S)$ production using different values of the wave function at the origin and two different UGDFs. Here $R(0) = 0.699\,\mathrm{GeV}^{3/2}$ is extracted from the experimental value for $\Gamma(\eta_c(1S) \to \gamma\gamma)$ [32] using the NLO expansion for Γ, whereas $R(0) = 0.762\,\mathrm{GeV}^{3/2}$ is the value obtained in ref. [15] for a power-law potential. The number relevant for describing $\Gamma(\eta_c(1S) \to \gamma\gamma)$ gives rather unsatisfactory distribution for each UGDFs, better agreement can be obtained using the form factor obtained with the help of the wave function (see figure 5).

In figure 12 we show the integrated cross section within the LHCb cuts for the three different energies measured up to now. In this plot we used the KMR UGD. We observe that the data appear to indicate a faster than linear rise of the cross section, while the
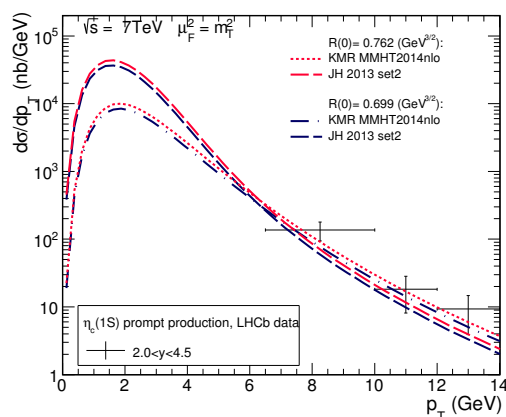
Figure 11. Differential cross section for prompt $\eta_c(1S)$ production in the NRQCD approach. $R(0) = 0.699\,\mathrm{GeV}^{3/2}$ is extracted from experimental radiation decay width using relation (2.45) from [15] and NLO expansion (see eq. (2.22)). For comparison, we also show the results for $R(0) = 0.762\,\mathrm{GeV}^{3/2}$ (the value which was obtained in [15] for power-law potential.
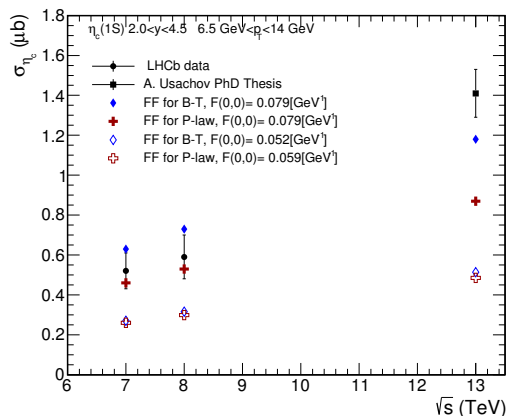

Figure 12. The integrated cross section computed within LHCb range of p_T and y with our transition form factors, compared to experimental values. Here red crosses represent values for Buchmüller-Tye potential (B-T) and deltoids for Power-law potential (P-law).

theoretical calculations predict a slightly slower rise of the cross section with $\sqrt{s}$. We checked that similar results are obtained with other UGDs. Once more we remind of the missing feed-down component. A possible color-octet component is not expected to change the energy dependence, as it is driven by the similar $g^*g^* \to c\bar{c}$ process.

It is interesting to investigate what is the role of the off-shell form factor. For example in the approach of ref. [23] gluon virtualities are neglected in the hard matrix element. The curves in figure 13 clearly show that the effect of the inclusion of gluon virtualities in the transition form factor is essential and cannot be neglected.

Up to now we concentrated on the kinematics of the LHCb experiment. Could η_c quarkonia be measured by other experiments at the LHC? In figure 14 we show the ranges of x_i and q_{Ti} carried by gluons for a rapidity interval $-2.5 < y < 2.5$ typical of the
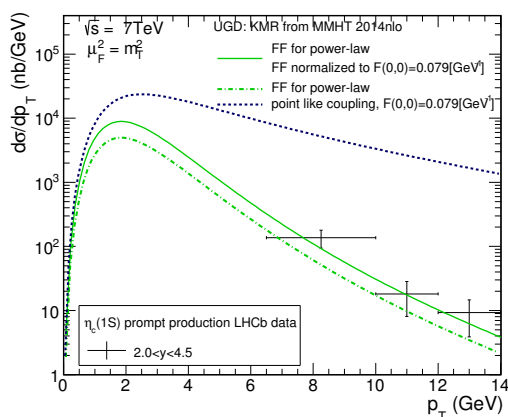
Figure 13. Comparison of results for two different transition form factor, computed with the KMR unintegrated gluon distribution. We also show result when the (q^2_{1T}, q^2_{2T}) dependence of the transition form factor is neglected.
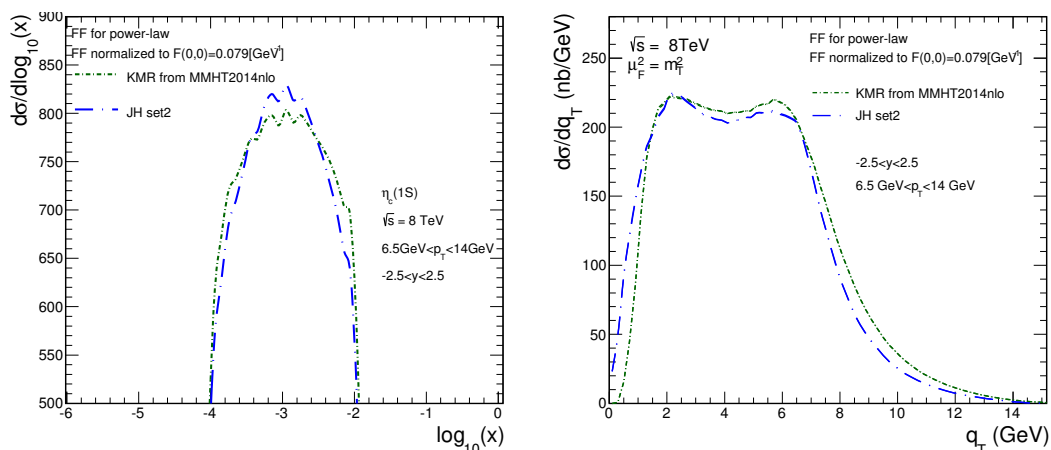

Figure 14. Distribution in $\log_{10}(x_1)$ or $\log_{10}(x_2)$ (left panel) and distribution in q_{1T} or q_{2T} (right panel) for ATLAS or CMS conditions.

central detectors of ATLAS or CMS. As in the case of LHCb, we assumed a lower cut on transverse momentum, $p_T > 6.5\,\mathrm{GeV}$. In the center-of-mass rapidity interval symmetric around zero, of course both UGDs enter symmetrically and therefore the distributions of x_1 and x_2 coincide, as do the ones for q_{1T} and q_{2T} We find that in the central rapidity region one would test $x_1, x_2 \sim 10^{-4}$ - 10^{-2} i.e. the region where the gluon is already known reasonably well from the HERA experiments. The q_{iT}-distribution has a large plateau at perturbatively large values, so that we suppose that the predictions of the KMR UGD should be reliable in this case.

The corresponding transverse momentum distributions are shown in figure 15 for two different UGDs reliable for this region of longitudinal momentum fractions and gluon transverse momenta. Notice that because there is some contribution of $x > 0.01$, we cannot use here the Kutak UGDs, which are unavailable at these x-values.
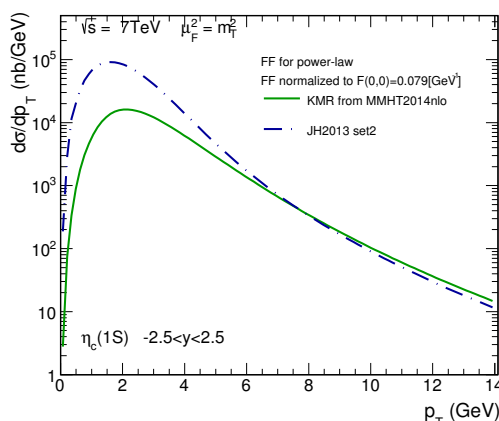
Figure 15. Transverse momentum distribution of prompt $\eta_c(1S)$ for $-2.5 < y < 2.5$ and $\sqrt{s} = 7\,\mathrm{TeV}$.

4 Conclusions

In the present paper we have discussed in detail the production of pseudoscalar η_c quarkonia in proton-proton collisions at the LHC energies. The calculations have been performed in the k_T-factorization approach using $g^* g^* \to \eta_c$ vertex calculated from the $c\bar{c}$ wave functions. The latter vertices are closely related to the $\gamma^* \gamma^* \to \eta_c$ transition form factors which were obtained recently in [15] and which we used in the present work.

We have used different unintegrated gluon distributions available in the literature: firstly the KMR UGD, which effectively includes higher-order effects of the collinear approach, secondly two UGDs by Kutak which were obtained by using linear and nonlinear small-x evolution equations, and thirdly the Jung-Hautmann UGD from 2013, obtained from a fit to HERA data in a CCFM approach.

We have calculated transverse momentum distributions of both $\eta_c(1S)$ and $\eta_c(2S)$ charmonia. The results of the $\eta_c(1S)$ have been compared with the experimental data obtained by the LHCb collaboration for $\sqrt{s} = 7, 8\,\mathrm{GeV}$ [13] and to a measurement at $\sqrt{s} = 13\,\mathrm{TeV}$ published in a PhD thesis [14].

A quite good agreement with the data was obtained with the KMR UGD. We have shown the range of x_1, x_2 and gluon transverse momenta q_{1T}, q_{2T} probed in the kinematics of the LHCb experiment [13, 14]. For the LHCb experiment one of the x-values, $x_1 \in (10^{-2}, 10^{-1})$ is large, while the second one, $x_2 \in (10^{-5}, 10^{-4})$ takes very small values. For the LHCb experiment we have shown also a large asymmetry in q_{1T} (larger) and q_{2T} (smaller). It turns out that at large p_T of the meson the bulk of transverse momenta is transferred by the small-x gluon. The Kutak UGD cannot be used for the range of x_1 relevant for the LHCb experiment. Therefore in this case we have used two different UGDs: Kutak UGD for small x_2 and KMR UGD for large x_1. We have used both the linear and nonlinear UGDs of Kutak. The mixed UGD scenario with the linear Kutak UGD leads to very similar transverse momentum distribution of η_c as that for using the KMR UGD on both sides. Indeed in the considered range of x and k_T the linear Kutak UGD is very

similar as the KMR UGD. The nonlinear version of the Kutak UGD leads to smaller cross sections, especially for small η_c transverse momenta.

A measurement of η_c at low transverse momenta in the LHCb kinematics would therefore be very valuable in the context of searching for nonlinear effects and onset of gluon saturation. One could, for example, consider another measurement for the $\gamma\gamma$ decay channel.

We have shown that it is crucial to include the dependence on gluon virtualities in the $g^*g^* \to \eta_c(1S, 2S)$ vertex. We have also discussed uncertainties related to the $g^*g^* \to \eta_c(1S,2S)$ form factor. We have shown results of calculations with the form factor obtained from different $c\bar{c}$ potentials from the literature. The associated uncertainty is somewhat smaller than that related to the choice of UGD. For comparison we have shown also result for the NRQCD approach, where internal motion of quarks is neglected. The agreement with the LHCb data cannot be obtained with $R(0)$ corresponding to experimental radiative decay with for $\eta_c(1S)$.

A better measurement of $\eta_c(1S,2S) \to \gamma\gamma$ would be important in this context.

Acknowledgments

References

[1] J.-P. Lansberg, *New observables in inclusive production of quarkonia*, [arXiv:1903.09185](#) [INSPIRE].

[2] L.V. Gribov, E.M. Levin and M.G. Ryskin, *Semihard processes in QCD*, [*Phys. Rept.* **100** (1983) 1](#) [INSPIRE].

[3] E.M. Levin et al. , *Heavy quark production in semihard nucleon interactions*, *Sov. J. Nucl. Phys.* **53** (1991) 657 [*Yad. Fiz.* **53** (1991) 1059] [INSPIRE].

[4] S. Catani, M. Ciafaloni and F. Hautmann, *Gluon contributions to small x heavy flavor production*, [*Phys. Lett.* **B 242** (1990) 97](#) [INSPIRE].

[5] S. Catani, M. Ciafaloni and F. Hautmann, *High-energy factorization and small x heavy flavor production*, [*Nucl. Phys.* **B 366** (1991) 135](#) [INSPIRE].

[6] S. Catani, M. Ciafaloni and F. Hautmann, *High-energy factorization in QCD and minimal subtraction scheme*, *Phys. Lett.* **B 307** (1993) 147 [INSPIRE].

[7] J.C. Collins and R.K. Ellis, *Heavy quark production in very high-energy hadron collisions*, *Nucl. Phys.* **B 360** (1991) 3 [INSPIRE].

[8] V.S. Fadin, E.A. Kuraev and L.N. Lipatov, *On the Pomeranchuk singularity in asymptotically free theories*, *Phys. Lett.* **B 60B** (1975) 50.

[9] I.I. Balitsky and L.N. Lipatov, *The Pomeranchuk Singularity in Quantum Chromodynamics*, *Sov. J. Nucl. Phys.* **28** (1978) 822 [INSPIRE].

[10] L.N. Lipatov, *Small x physics in perturbative QCD*, *Phys. Rept.* **286** (1997) 131 [hep-ph/9610276] [INSPIRE].

[11] E.N. Antonov, L.N. Lipatov, E.A. Kuraev and I.O. Cherednikov, *Feynman rules for effective Regge action*, *Nucl. Phys.* **B 721** (2005) 111 [hep-ph/0411185] [INSPIRE].

[12] A. Cisek and A. Szczurek, *Prompt inclusive production of J/ψ, ψ' and χ_c mesons at the LHC in forward directions within the NRQCD k_t-factorization approach — Search for the onset of gluon saturation*, *Phys. Rev.* **D 97** (2018) 034035 [arXiv:1712.07943] [INSPIRE].

[13] LHCb collaboration, *Measurement of the $\eta_c(1S)$ production cross-section in proton-proton collisions via the decay $\eta_c(1S) \to p\bar{p}$*, *Eur. Phys. J.* **C 75** (2015) 311 [arXiv:1409.3612] [INSPIRE].

[14] A. Usachov, *Study of charmonium production using decays to hadronic final states with the LHCb experiment*, Ph.D. thesis, U. Paris-Saclay, 2019. arXiv:1910.08796 [INSPIRE].

[15] I. Babiarz et al., *$\gamma^*\gamma^* \to \eta_c(1S, 2S)$ transition form factors for spacelike photons*, *Phys. Rev.* **D 100** (2019) 054018 [arXiv:1908.07802] [INSPIRE].

[16] J. Cepila, J. Nemchik, M. Krelina and R. Pasechnik, *Theoretical uncertainties in exclusive electroproduction of S-wave heavy quarkonia*, *Eur. Phys. J.* **C 79** (2019) 495 [arXiv:1901.02664] [INSPIRE].

[17] M. Krelina, J. Nemchik and R. Pasechnik, *D-wave effects in diffractive electroproduction of heavy quarkonia from the photon-like $V \to Q\bar{Q}$ transition*, arXiv:1909.12770 [INSPIRE].

[18] D. Diakonov, M.G. Ryskin and A.G. Shuvaev, *Gluon distribution at very small x from C-even charmonia production at the LHC*, *JHEP* **02** (2013) 069 [arXiv:1211.1578] [INSPIRE].

[19] A.K. Likhoded, A.V. Luchinsky and S.V. Poslavsky, *Production of η_Q meson at LHC*, *Mod. Phys. Lett.* **A 30** (2015) 1550032 [arXiv:1411.1247] [INSPIRE].

[20] M. Butenschoen, Z.-G. He and B.A. Kniehl, *η_c production at the LHC challenges nonrelativistic-QCD factorization*, *Phys. Rev. Lett.* **114** (2015) 092004 [arXiv:1411.5287] [INSPIRE].

[21] H.-F. Zhang, Z. Sun, W.-L. Sang and R. Li, *Impact of η_c hadroproduction data on charmonium production and polarization within NRQCD framework*, *Phys. Rev. Lett.* **114** (2015) 092006 [arXiv:1412.0508] [INSPIRE].

[22] Y. Feng et al., *Phenomenological NLO analysis of η_c production at the LHC in the collider and fixed-target modes*, *Nucl. Phys.* **B 945** (2019) 114662 [arXiv:1901.09766] [INSPIRE].

[23] D. Boer and C. Pisano, *Polarized gluon studies with charmonium and bottomonium at LHCb and AFTER*, *Phys. Rev.* **D 86** (2012) 094007 [arXiv:1208.3642] [INSPIRE].

[24] M.G. Echevarria, *Proper TMD factorization for quarkonia production: $pp \to \eta_{c,b}$ as a study case*, *JHEP* **10** (2019) 144 [`arXiv:1907.06494`] [ɪɴSPIRE].

[25] S.P. Baranov and A.V. Lipatov, *Prompt η_c meson production at the LHC in the NRQCD with k_T-factorization*, *Eur. Phys. J.* **C 79** (2019) 621 [`arXiv:1904.00400`] [ɪɴSPIRE].

[26] J.-P. Lansberg, H.-S. Shao and H.-F. Zhang, *η_c' hadroproduction at next-to-leading order and its relevance to ψ' production*, *Phys. Lett.* **B 786** (2018) 342 [`arXiv:1711.00265`] [ɪɴSPIRE].

[27] J.P. Lansberg and T.N. Pham, *Two-photon width of η_c and η_c' from heavy-quark spin symmetry*, *Phys. Rev.* **D 74** (2006) 034001 [`hep-ph/0603113`] [ɪɴSPIRE].

[28] J.P. Lansberg and T.N. Pham, *Effective Lagrangian for two-photon and two-gluon decays of P-wave heavy quarkonium $\chi(c_0, 2)$ and $\chi(b_0, 2)$ states*, *Phys. Rev.* **D 79** (2009) 094016 [`arXiv:0903.1562`] [ɪɴSPIRE].

[29] M.A. Shifman, A.I. Vainshtein, M.B. Voloshin and V.I. Zakharov, *η_c puzzle in quantum chromodynamics*, *Phys. Lett.* **B 77** (1978) 80.

[30] N. Kochelev and D.-P. Min, *Eta(c): Glueball mixing and resonance X(1835)*, *Phys. Rev.* **D 72** (2005) 097502 [`hep-ph/0510016`] [ɪɴSPIRE].

[31] V. Zetocha and T. Schäfer, *Instanton contribution to scalar charmonium and glueball decays*, *Phys. Rev.* **D 67** (2003) 114003 [`hep-ph/0212125`] [ɪɴSPIRE].

[32] PARTICLE DATA GROUP collaboration, *Review of particle physics*, *Phys. Rev.* **D 98** (2018) 030001.

[33] F. Hautmann et al., *TMDlib and TMDplotter: library and plotting tools for transverse-momentum-dependent parton distributions*, *Eur. Phys. J.* **C 74** (2014) 3220 [`arXiv:1408.3015`] [ɪɴSPIRE].

[34] H. Jung et al., *The CCFM Monte Carlo generator CASCADE version 2.2.03*, *Eur. Phys. J.* **C 70** (2010) 1237 [`arXiv:1008.0152`] [ɪɴSPIRE].

[35] M.A. Kimber, A.D. Martin and M.G. Ryskin, *Unintegrated parton distributions*, *Phys. Rev.* **D 63** (2001) 114027 [`hep-ph/0101348`] [ɪɴSPIRE].

[36] A.D. Martin, M.G. Ryskin and G. Watt, *NLO prescription for unintegrated parton distributions*, *Eur. Phys. J.* **C 66** (2010) 163 [`arXiv:0909.5529`] [ɪɴSPIRE].

[37] G. Watt, A.D. Martin and M.G. Ryskin, *Unintegrated parton distributions and electroweak boson production at hadron colliders*, *Phys. Rev.* **D 70** (2004) 014012 [*Erratum ibid.* **D 70** (2004) 079902] [`hep-ph/0309096`] [ɪɴSPIRE].

[38] L.A. Harland-Lang, A.D. Martin, P. Motylinski and R.S. Thorne, *Parton distributions in the LHC era: MMHT 2014 PDFs*, *Eur. Phys. J.* **C 75** (2015) 204 [`arXiv:1412.3989`] [ɪɴSPIRE].

[39] K. Kutak, *Hard scale dependent gluon density, saturation and forward-forward dijet production at the LHC*, *Phys. Rev.* **D 91** (2015) 034021 [`arXiv:1409.3822`] [ɪɴSPIRE].

[40] I. Balitsky, *Operator expansion for high-energy scattering*, *Nucl. Phys.* **B 463** (1996) 99 [`hep-ph/9509348`] [ɪɴSPIRE].

[41] Y.V. Kovchegov, *Small x F_2 structure function of a nucleus including multiple Pomeron exchanges*, *Phys. Rev.* **D 60** (1999) 034008 [`hep-ph/9901281`] [ɪɴSPIRE].

[42] Y.V. Kovchegov, *Unitarization of the BFKL Pomeron on a nucleus*, *Phys. Rev.* **D 61** (2000) 074018 [`hep-ph/9905214`] [ɪɴSPIRE].

[43] F. Hautmann and H. Jung, *Transverse momentum dependent gluon density from DIS precision data*, *Nucl. Phys.* **B 883** (2014) 1 [arXiv:1312.7875] [ɪɴSPIRE].

[44] M. Ciafaloni, *Coherence effects in initial jets at small Q^2/s*, *Nucl. Phys.* **B 296** (1988) 49 [ɪɴSPIRE].

[45] S. Catani, F. Fiorani and G. Marchesini, *QCD Coherence in Initial State Radiation*, *Phys. Lett.* **B 234** (1990) 339 [ɪɴSPIRE].

[46] S. Catani, F. Fiorani and G. Marchesini, *Small x behavior of initial state radiation in perturbative QCD*, *Nucl. Phys.* **B 336** (1990) 18 [ɪɴSPIRE].

[47] R. Maciula and A. Szczurek, *Consistent treatment of charm production in higher-orders at tree-level within k_T-factorization approach*, *Phys. Rev.* **D 100** (2019) 054001 [arXiv:1905.06697] [ɪɴSPIRE].

[48] Z. Metreveli, *Charmonium spectroscopy below open flavor threshold*, *eConf* **C 070805** (2007) 16 [arXiv:0710.1884] [ɪɴSPIRE].